Prepared for submission to JCAP

APCTP-PRE2015-015

Prospects for higgsino-singlino dark matter detection at IceCube and PINGU

R. Enberg,[a] **S. Munir,**[a,b] **C. Pérez de los Heros**[a] **and D. Werder**[a]

[a]Department of Physics and Astronomy, Uppsala University,
Box 516, SE–751 20 Uppsala, Sweden

[b]Asia Pacific Center for Theoretical Physics, San 31, Hyoja-dong,
Nam-gu, Pohang 790-784, Republic of Korea

E-mail: rikard.enberg@physics.uu.se, s.munir@apctp.org, cph@physics.uu.se,
dominik.werder@physics.uu.se

Abstract. We study neutralino dark matter (DM) with large singlino fractions in the next-to-minimal supersymmetric Standard Model (NMSSM). We perform a detailed analysis of the parameter space regions of the model that give rise to such singlino-dominated neutralinos while satisfying the constraints from Higgs boson searches at the Large Electron Positron (LEP) collider and the Large Hadron Collider (LHC), as well as from b-physics experiments. We find that this DM can yield a thermal relic density consistent with the Planck measurement in mass regions where the lightest neutralino of the minimal supersymmetric Standard Model (MSSM) generally cannot. This is particularly true for lighter DM masses, either less than 10 GeV or between $60 - 100$ GeV, and for heavier DM masses, between $500 - 1000$ GeV. We then analyse the prospects for indirect detection of such DM at the IceCube neutrino telescope, assuming the complete 86-string configuration including DeepCore. We also consider the added sensitivity to low-mass DM with the proposed PINGU extension. We find that IceCube is sensitive to some regions of the NMSSM parameter space containing singlino-dominated DM and that a subset of such model points are already ruled out by the IceCube one-year data. IceCube will also be sensitive to some parameter space regions that will not be probed by the upcoming ton-scale direct detection experiments. Moreover, we find that PINGU will be sensitive to DM in the 10 GeV range.

Contents

1 Introduction

The nature of the dark matter of the Universe is one of the major unresolved problems in physics. Supersymmetric models with unbroken R-parity provide a possible candidate for a weakly interacting massive particle (WIMP), the lightest neutralino, which has been studied extensively (see e.g. [1–4]). There are good phenomenological and theoretical reasons apart from the DM problem to consider such supersymmetric (SUSY) extensions of the Standard Model (SM), including amelioration of the hierarchy problem or the fine-tuning of the Higgs boson mass and unification of the gauge couplings.

The most commonly studied SUSY model is the MSSM [5, 6], which exhibits all of the above benefits. The price for these benefits is a common mass term (called the μ-term) for the two Higgs doublets of the MSSM. This leads to another fine-tuning problem, namely why the μ parameter should lie at the electroweak (EW) scale, as is required by phenomenology, when its natural value would be the Planck scale. This is known as the μ-problem. Furthermore, the mass of the lightest Higgs boson in the MSSM at the tree level has an upper limit equal to the Z boson mass. To fulfil the experimental constraints, large corrections to the Higgs mass from the stop (and top) loops are needed, which require a rather large stop mass, leading to an additional source of fine-tuning in the model. If we take fine-tuning arguments seriously, we may consider exploring alternatives to the MSSM.

One such alternative is the NMSSM [7–10], which has been reviewed in Refs. [11, 12]. In the NMSSM, in addition to the two Higgs doublets of the MSSM there is a singlet Higgs field, which is the scalar component of a chiral singlet superfield added to the MSSM superpotential. The reason for introducing this additional scalar is that an effective μ-term is now dynamically generated, so that the fine-tuned parameter μ is no longer needed (and can be removed by imposing a discrete Z_3 symmetry). This new scalar mixes with the other scalars from the two doublets, leading to a Higgs sector with seven Higgs bosons, compared to the five present in the MSSM. In addition, the fermion component of the singlet superfield, the singlino, mixes

with the higgsinos and gauginos, the fermion components of the Higgs doublet and gauge superfields, respectively, resulting in a total of five neutralinos.

The interaction strengths of the neutralinos with other SM and SUSY particles are governed by their masses and compositions. In the MSSM, the neutralinos are broadly classified as gaugino-like, higgsino-like and mixed gaugino-higgsino states, depending on the relative sizes of the soft SUSY-breaking gaugino mass parameters, $M_{1,2}$, and the μ -parameter in the neutralino mass matrix. If $M_{1,2}$ are much larger than μ, two of the neutralinos are predominantly higgsino-like and the other two are gaugino-dominated, while a smaller difference results in larger gaugino-higgsino mixing. Similarly, in the NMSSM, the fifth neutralino is either completely singlino-dominated or can be an admixture of the singlino and, chiefly, the higgsinos. This purely singlino or mixed higgsino-singlino state can be the lightest of the five neutralinos and hence the lightest supersymmetric particle (LSP) after diagonalisation of the mass matrix. If so, some interesting possibilities arise in the context of DM phenomenology, which are rather distinct from the MSSM. In particular, such a neutralino can give the correct DM relic abundance with a considerably smaller mass [13–17] than is generally possible for the lightest neutralino in the MSSM, given the LHC exclusion limits on SUSY.

A light singlino-dominated neutralino LSP in the NMSSM has been the subject of several studies recently. It is an important candidate for the events near $\sim 10\,\text{GeV}$ [14, 15] reported by the CDMS II Collaboration [18]. With a mass near 35 GeV, such a neutralino can also explain [19–22] the $\sim 1-4\,\text{GeV}$ γ-ray excess from the galactic centre reported by the Fermi Large Area Telescope (LAT) [23, 24] (for most recent results from Fermi-LAT, see [25]). Generally, the existence of a light DM candidate is also supported by some other direct detection experiments such as DAMA/LIBRA [26], CoGeNT [27, 28] and CRESST-II [29]. Experiments such as XENON100 [30], LUX [31] or PICO [32] have released strong exclusion constraints on the interaction strength of a generic DM candidate with a nucleon for a considerably wide range of its mass. Signatures of a higgsino-singlino LSP that can be probed at the LHC have been studied in [33–37]. Indirect detection prospects for neutralino DM in the NMSSM have been studied in [38, 39].

In this article we revisit the neutralino sector of the NMSSM, focusing on the LSP with a significant singlino fraction, which can give sufficient relic abundance in the Universe. Through scans of the NMSSM parameter space, which were subject to the most important experimental constraints, we find its regions where such neutralino solutions are realisable. We then analyse the potential of the IceCube neutrino telescope [40] to discover or exclude such LSP solutions. The annihilation of neutralinos captured in the centre of the Sun results in a neutrino flux at Earth. These neutrinos interact with ice at the South Pole, producing leptons which emit Cherenkov radiation that can be detected by IceCube. We take into account the winter data from a complete 86-string configuration of IceCube, i.e., including also the DeepCore strings, in order to perform a signal-to-background analysis of the good higgsino-singlino solutions obtained from our scans. The impact of the proposed extension PINGU [41] on the statistical significance for mainly low mass DM is also investigated in detail.

The article is organised as follows. In section 2 we discuss the NMSSM and its neutralino sector. In section 3 we provide details of the model's parameter space of interest, the procedure adopted for its scanning, the constraints imposed during these scans and the impact of these constraints. In section 4 we explain the neutrino flux from the Sun due to the annihilation of DM there. In section 5 we highlight some important features of the IceCube

neutrino observatory. In section 6 we present the details of the reconstruction of neutrinos from the Sun and the background for this signal at the IceCube. In section 7 we discuss the statistical treatment of the signal process and the sensitivity that can be reached at the IceCube after a given period of data accumulation. In section 8 we summarise our findings.

2 The neutralino sector of the NMSSM

The Z_3-symmetric CP-conserving NMSSM has no mass parameters in the superpotential, and is therefore also referred to as the scale-invariant NMSSM. It differs from the MSSM by the omission of the μ-term from the superpotential and the introduction of a singlet chiral superfield $\widehat{S}$, while the Yukawa terms remain unchanged. The superpotential is written as

$$W_{\text{NMSSM}} = W_{\text{Yukawa}} + \lambda \widehat{S} \widehat{H}_u \widehat{H}_d + \frac{\kappa}{3} \widehat{S}^3 \,, \tag{2.1}$$

where $\widehat{H}_u$ and $\widehat{H}_d$ are the two Higgs doublet superfields of the MSSM. The scalar potential of the NMSSM constitutes of the D-terms, which are the same as in the MSSM since S does not couple to the gauge bosons, the F-terms, plus the soft SUSY-breaking terms for the Higgs sector, which are given by

$$V_{\text{soft}} = m_{H_u}^2 |H_u|^2 + m_{H_d}^2 |H_d|^2 + m_S^2 |S|^2 + \left[\lambda A_\lambda S H_u H_d + \frac{1}{3} \kappa A_\kappa S^3 + \text{h.c.} \right] . \tag{2.2}$$

The NMSSM scalar potential contains the new parameters $\lambda, \kappa, A_\lambda, A_\kappa$, and m_S compared to the MSSM. The parameters $m_{H_u}^2$, $m_{H_d}^2$ and m_S^2 are related to the Z boson mass, m_Z, $\tan\beta \equiv v_u/v_d$, where v_u and v_d are the vacuum expectation values (VEVs) of H_u and H_d, respectively, and s, the VEV of the singlet field, through the minimisation conditions of the scalar potential for EW symmetry breaking, and can therefore be eliminated. Here, instead of s we will use the effective μ-term, $\mu_{\text{eff}} = \lambda s$, as a free parameter. The VEVs of the doublet Higgs fields also satisfy the relation $v_u^2 + v_d^2 = v^2 = 2m_W^2/g_2^2 = (174\,\text{GeV})^2$, where m_W is the mass of the W boson and g_2 is the $SU(2)_L$ gauge coupling.

The free parameters of the MSSM Higgs sector include m_A, the mass of the CP-odd scalar, $\tan\beta$ and μ. In the NMSSM m_A, which is the 1×1 entry of the pseudo-scalar mass matrix before diagonalisation, gets traded for A_λ and μ gets replaced by μ_{eff}, so that all in all we have six Higgs sector parameters $(\lambda, \kappa, A_\lambda, A_\kappa, \tan\beta, \mu_{\text{eff}})$. There are thus three more parameters in the NMSSM than in the MSSM, all of which originate in the Higgs sector.

As S is a complex field, there are two additional physical Higgs bosons in the NMSSM compared to the MSSM. For a CP-conserving Higgs sector (as is assumed here), we have three CP-even neutral states H_1, H_2, H_3 and two CP-odd neutral states A_1 and A_2, where we take the states to be ordered in mass, so that H_1 and A_1 are the lightest scalar and pseudo-scalar states, respectively.

The fermion component of $\widehat{S}$ is called the singlino, $\widetilde{S}$, which mixes with the gauginos, $\widetilde{B}^0$ and $\widetilde{W}_3^0$, and the higgsinos, $\widetilde{H}_d^0$ and $\widetilde{H}_u^0$. There are therefore five neutralinos in the NMSSM. At leading order the neutralino masses and mixings depend on the parameters of the neutralino mass matrix. If we introduce the vector $\widetilde{\psi}^0 = (-\text{i}\widetilde{B}^0, -\text{i}\widetilde{W}_3^0, \widetilde{H}_d^0, \widetilde{H}_u^0, \widetilde{S})$, the non-diagonal mass Lagrangian in the gauge eigenstate basis is given by

$$\mathcal{L}_{\text{mass}} = -\frac{1}{2} (\widetilde{\psi}^0)^T \mathcal{M}_{\widetilde{\chi}^0} \widetilde{\psi}^0 + \text{h.c.} \,, \tag{2.3}$$

where $\mathcal{M}_{\widetilde{\chi}^0}$ is the symmetric matrix

$$\mathcal{M}_{\widetilde{\chi}^0} = \begin{pmatrix} M_1 & 0 & -\frac{g_1 v_d}{\sqrt{2}} & \frac{g_1 v_u}{\sqrt{2}} & 0 \\ & M_2 & \frac{g_2 v_d}{\sqrt{2}} & -\frac{g_2 v_u}{\sqrt{2}} & 0 \\ & & 0 & -\mu_{\rm eff} & -\lambda v_u \\ & & & 0 & -\lambda v_d \\ & & & & 2\kappa s \end{pmatrix}, \tag{2.4}$$

with g_1 being the $U(1)_Y$ gauge coupling.

The neutralino masses and compositions at the tree level thus depend on the Higgs sector parameters $\lambda, \kappa, \mu_{\rm eff}, v_u, v_d$ and the gaugino masses M_1 and M_2. The mass matrix in eq. (2.4) can be diagonalised by a unitary matrix N to give $D = \mathrm{diag}(m_{\widetilde{\chi}^0_i}) = N^* \mathcal{M}_{\widetilde{\chi}^0} N^\dagger$, for $i = 1 - 5$. If all the parameters in the mass matrix are real (which we assume to be the case here) then the matrix N is orthogonal, and we have $D = N \mathcal{M}_{\widetilde{\chi}^0} N^T$. The neutralino mass eigenstates are then given by $\widetilde{\chi}^0_i = N_{ij} \widetilde{\psi}^0_j$.

The eigenvalues of N_{ij} are all real, but can be positive or negative. (They can be made positive by a phase transformation.) They are not ordered in mass after performing the diagonalisation, but should then be reordered so that $\widetilde{\chi}^0_1$ is the lightest neutralino. The linear combination,

$$\widetilde{\chi}^0_1 = N_{11} \widetilde{B}^0 + N_{12} \widetilde{W}^0_3 + N_{13} \widetilde{H}^0_d + N_{14} \widetilde{H}^0_u + N_{15} \widetilde{S}^0 \,, \tag{2.5}$$

is thus our DM candidate. In order to describe the composition of $\widetilde{\chi}^0_1$, we define the gaugino fraction in it as $Z_g = |N_{11}|^2 + |N_{12}|^2$, the higgsino fraction as $Z_h = |N_{13}|^2 + |N_{14}|^2$ and the singlino fraction as $Z_s = |N_{15}|^2$. As noted earlier, the focus of this study is a $\widetilde{\chi}^0_1$ with a non-negligible singlino fraction, which we define to be $Z_s \geq 0.05$. Such a $\widetilde{\chi}^0_1$ could lead to some distinct phenomenological scenarios precluded in the MSSM.

Let us note some properties of the tree-level neutralino mass matrix given in eq. (2.4), assuming the mass parameters M_1 and M_2 of the gauginos to be very heavy so that they are decoupled from the 3×3 higgsino-singlino block. The 5×5 diagonal element, $2\kappa s = 2\kappa \mu_{\rm eff}/\lambda$, corresponds to the mass of the singlino. Thus, if this is small the $\widetilde{\chi}^0_1$ is more likely to be singlino-dominated after diagonalisation. Similarly, if $\mu_{\rm eff}$ is small, depending on the size of λ, the lightest neutralino can instead have a larger higgsino component. To have a singlino-dominated WIMP, we therefore need a large $\mu_{\rm eff}$ and a small κ. A large λ also reduces the size of the 5×5 term, but at the same time it enhances the sizes of the off-diagonal terms, leading to a larger mixing. Note, however, that the presence of a certain amount of higgsino in the WIMP is necessary to obtain a realistic relic abundance. Thus $\mu_{\rm eff}$ should not be too large and λ should not be too small. Evidently, the composition of such a WIMP is quite insensitive to the value of $\tan\beta$. In reality the situation is more complex, as the other elements of the matrix also need to be considered. Moreover, just as in the MSSM, this mass matrix is subject to radiative corrections [42–49] from various other sectors of the NMSSM. Thus, at higher orders the parameters of these sectors also become crucial.

3 Model scans and constraints

As noted above, beyond tree level the parameters of other SUSY sectors also need to be taken into account along with the Higgs sector ones, when drawing inferences about the neutralino sector. However, the most general EW-scale NMSSM contains more than 130

parameters in total. One way to reduce the number of free parameters is to consider a minimal supergravity-like scenario in which all the dimensional parameters are defined at the grand unification (GUT) scale and certain universality conditions are imposed on them. In this so-called constrained NMSSM (CNMSSM) (for some recent analyses, see, e.g., [50–52]) the scalar soft SUSY-breaking masses are unified into a generic mass parameter m_0, the gaugino masses into $m_{1/2}$, and all the trilinear couplings into a_0. Then, given m_Z, these three parameters along with the coupling λ, taken as an input at the SUSY-breaking scale, $M_{\rm SUSY}$, and the sign of $\mu_{\rm eff}$ constitute the only free parameters. All the parameters at $M_{\rm SUSY}$ are then obtained from these GUT-scale parameters using the renormalisation group equations.

In order to allow more freedom in adjusting the Higgs and neutralino sector parameters, one can relax the above-mentioned universality conditions partially. In that case, similarly to the MSSM with non-universal Higgs masses (NUHM), m_{H_u}, m_{H_d} and m_S are disunified from m_0 at the GUT scale and taken as free parameters, which can then be traded for κ, $\mu_{\rm eff}$ and $\tan\beta$ at the EW scale. Also, a_λ and a_κ, the GUT-scale input values, respectively, of the EW-scale parameters A_λ and A_κ, are disunified from a_0. This results in a total of nine input parameters and we refer to this model as the next-to-NUHM (NNUHM) here.

Alternatively, without imposing the GUT-universality conditions, a convenient way to considerably reduce the number of parameters in the general EW-scale NMSSM is to assume that the matrices for the sfermion masses and for the trilinear scalar couplings are diagonal. Furthermore, the soft SUSY-breaking parameters are taken to be real and those corresponding to the first two generations are unified. Thus, with only about 25 or so parameters in total, one can study the most important low-energy characteristics of the model. In our analysis, while requiring the $\widetilde{\chi}_1^0$ to have $Z_s \geq 0.05$, we also want to take into account all of its possible annihilation and co-annihilation channels resulting in the correct relic abundance. Some of these co-annihilation channels require the existence of a sfermion not much heavier than the $\widetilde{\chi}_1^0$ itself. However, in order that the model candidate for the SM-like Higgs boson, $H_{\rm obs}$, observed at the LHC [53–55] has a mass near 125 GeV, large corrections from the SUSY sector are necessary, implying sufficiently large sfermion mass parameters. Crucially though, these corrections are almost entirely dominated by the stops. In view of all these considerations, we impose the following universality conditions on the parameters of the general NMSSM:

$$
\begin{aligned}
M_{\widetilde{Q}} \equiv M_{\widetilde{Q}_{1,2}} = M_{\widetilde{U}_{1,2}} = M_{\widetilde{D}_{1,2}}\,, \\
M_{\widetilde{L}} \equiv M_{\widetilde{L}_{1,2,3}} = M_{\widetilde{E}_{1,2,3}}\,, \\
M_2 = \frac{1}{3} M_3\,, \\
A_0 \equiv A_t = A_b = A_\tau\,,
\end{aligned}
$$

where $M_{Q_{1,2}}$, $M_{U_{1,2}}$, $M_{D_{1,2}}$ are the soft masses of the squarks from the first two generations, $M_{L_{1,2,3}}$ and $M_{E_{1,2,3}}$ the soft slepton masses, $M_{1,2,3}$ the soft gaugino masses and $A_{t,b,\tau}$ the trilinear Higgs-sfermion couplings.[1] This leaves us with a total of 14 free parameters to scan over. In the following we will refer to this model as the NMSSM-14.

In order to obtain maximum possible configurations of the free parameters that yield the desired neutralino composition while satisfying important constraints coming from various

[1] Note in particular that a unique soft mass has been used for all three generations of the sleptons. This is not the case for the squarks, for which the soft masses of the first two generations are disunified from the respective ones, $M_{\widetilde{Q}_3}$, $M_{\widetilde{U}_3}$ and $M_{\widetilde{D}_3}$, of the third generation.

experimental sources, these parameters need to be scanned numerically. We first carried out scans for the NNUHM, using the MultiNest-v2.18 [56] package, which is linked to the public code NMSSMTools-v4.2.1 [57–60] to calculate the SUSY mass spectra and branching ratios (BRs) as well as the Higgs boson signal rates. The signal rate is defined, for the X decay channel of a given NMSSM Higgs boson, H_i, as

$$R_i^X \equiv \frac{\sigma(gg \to H_i) \times \mathrm{BR}(H_i \to X)}{\sigma(gg \to h_{\mathrm{SM}}) \times \mathrm{BR}(h_{\mathrm{SM}} \to X)}\,, \tag{3.1}$$

where h_{SM} is the SM Higgs boson with the same mass as H_i.

We consider two distinct scenarios for the Higgs sector: one scenario where the H_{obs} corresponds to the lightest NMSSM Higgs boson, H_1, and one where the H_{obs} corresponds to the heavier H_2. In the latter scenario, there is thus a Higgs boson with mass less than 125 GeV that remains to be discovered. Both of these scenarios are easily realisable in significant portions of the NMSSM parameter space [61–66]. Separate scans were performed for the NNUHM for these two scenarios. A H_i, with $i = 1, 2$, is identified with the H_{obs} by requiring it to have a mass lying in the $122 - 128$ GeV range[2] and R^X_{obs} consistent with the experimentally measured $\mu^X \equiv \sigma(pp \to H_{\mathrm{obs}} \to X)/\sigma(pp \to h_{\mathrm{SM}} \to X)$ within $\pm 1\sigma$ error, for each X. This condition assumes that the inclusive pp cross section for Higgs boson production at the LHC can be approximated by the dominant gluon fusion channel. Note, however, that in the rare cases when $\sigma(gg \to H_{\mathrm{obs}} \to X)/\sigma(gg \to h_{\mathrm{SM}} \to X)$ for a given X is also provided by the experimental collaboration, we use it instead as μ^X for comparing R^X_{obs} with.

The most recent publicly released values of μ^X measured by the ATLAS and CMS collaborations are given in table 1. Instead of considering the two sets of experimental measurements of the same observables separately in two scans for the given H_{obs} case, we delineate an 'optimal allowed range' of each R^X_{obs}. This range spans $\min[\mu^X - |1\sigma|^\vee\,(\mathrm{ATLAS}), \mu^X - |1\sigma|^\vee\,(\mathrm{CMS})]$ to $\max[\mu^X + |1\sigma|^\wedge\,(\mathrm{ATLAS}), \mu^X + |1\sigma|^\wedge\,(\mathrm{CMS})]$, where μ^X denotes the central value of the measurement and $|1\sigma|^\wedge$ and $|1\sigma|^\vee$ imply, respectively, the positive and negative error on it, as long as $\mu^X - |1\sigma|^\wedge$ for one experiment is not higher than $\mu^X - |1\sigma|^\vee$ for the other. This range is also given in the last column of table 1 for each X. One can notice in the table that while $\mu^{\gamma\gamma}$ from the two collaborations are mutually consistent, the ATLAS measurement of μ^{ZZ} is considerably higher than the CMS one. Note also that since the WW and ZZ decays of a given H_i depend on the same VVH_i reduced coupling, NMSSMTools computes a unique value, R^{VV}_{obs}, of the signal rates for both these channels. Therefore, our defined optimal range of R^{VV}_{obs} covers $\mu^{ZZ} - |1\sigma|^\vee$ from CMS to $\mu^{WW} + |1\sigma|^\wedge$ from ATLAS. We ignore the μ^{bb} measurement here since, aside from the fact that the error on it is very large, it does not take into account the gluon fusion mode for the production of H_{obs}.

During our scans the b-physics observables were subject to the following constraints.

- $2.63 \times 10^{-4} \leq \mathrm{BR}\left(\overline{\mathrm{B}} \to \mathrm{X_s}\gamma\right) \leq 4.23 \times 10^{-4}$ [71–73],
- $0.71 \times 10^{-4} < \mathrm{BR}\left(\mathrm{B_u} \to \tau\nu\right) < 2.57 \times 10^{-4}$ [71–73],
- $1.3 \times 10^{-9} < \mathrm{BR}\left(\mathrm{B_s} \to \mu^+\mu^-\right) < 4.5 \times 10^{-9}$ [74–76].

The theoretical evaluation of these observables was carried out using SuperIso-v3.4 [77] and the above ranges are the ones allowed at the 95% confidence level (CL), as suggested

[2]The extended mass range is to allow up to 3 GeV uncertainty in the theoretical prediction of the mass of the assumed H_{obs}.

X	μ^X(CMS) [67]	μ^X(ATLAS)	Allowed $R^X_{\rm obs}$ range	Observed $R^X_{\rm obs}$ range	
				$H_{\rm obs} = H_1$	$H_{\rm obs} = H_2$
$\gamma\gamma$	1.13 ± 0.24	1.17 ± 0.27 [68]	0.89 – 1.37	0.91 – 1.1	0.89 – 1.12
ZZ	1.0 ± 0.29	$1.44^{+0.40}_{-0.35}$ [69]	0.71 – 1.31	0.95 – 1.05	0.88 – 1.05
WW	0.83 ± 0.21	$1.09^{+0.23}_{-0.21}$ [70]			
$\tau\tau$	0.91 ± 0.28	$1.4^{+0.5}_{-0.4}$ [69]	0.63 – 1.9	0.9 – 1.01	0.63 – 1.06

Table 1: Higgs boson signal rates measured by the CMS and ATLAS collaborations, their ranges enforced in the scans and those observed for the good points from the scans corresponding to the $H_{\rm obs} = H_1$ and $H_{\rm obs} = H_2$ cases.

in the manual of the package. Each SUSY point was also required to be consistent with the LEP and LHC exclusion limits on the other, non-SM-like, Higgs bosons of the model, as tested using HiggsBounds-v4.1.3 [78–81]. The satisfaction of the LEP limit on $\widetilde{\chi}_1^+$ mass and the perturbativity constraints on the various Higgs boson couplings are ensured by NMSSMTools intrinsically. While it also tests each point against the squark/gluino and slepton searches from the LHC, for added surety we further required the scan to allow a point only if it gave a gluino mass larger than 1400 GeV. Finally, we enforced an upper limit on the $\widetilde{\chi}_1^0$ thermal relic density, $\Omega_{\widetilde{\chi}_1^0}h^2$, to be less than 0.131, thus allowing up to +10% error in its theoretical calculation (and in this way taking into account also the experimental error), performed by the package MicrOMEGAs-v4.1.5 [82], given the measured value of 0.119 from the Planck telescope [83, 84]. No lower limit is imposed on $\Omega_{\widetilde{\chi}_1^0}h^2$ in view of the possibility that $\widetilde{\chi}_1^0$ can make up 100% of the DM in the universe via, e.g., non-thermal production [85], despite yielding an under-abundant thermal relic density. There is also the alternative possibility of the $\widetilde{\chi}_1^0$ constituting only a fraction of a multi-component DM (see, e.g., [86]).

Our scans showed that the NNUHM serves as a good approximation for the general NMSSM for the $H_{\rm obs} = H_2$ scenario, since we obtained a sufficiently large number of points with the desired neutralino composition. We point out here that in this scenario, the H_2 can obtain a large tree-level mass in a more 'natural' way, i.e., without requiring very large corrections from the SUSY sectors and hence forcing sparticle masses to be large, for its physical mass to lie near 125 GeV. This happens for $\lambda \gtrsim 0.1$ and $\tan\beta$ not too large. The scanned ranges of the input parameters were chosen in light of these observations, and are listed in table 2(a). Also, in this scenario the $\widetilde{\chi}_1^0$, typically a higgsino-singlino mixture, is generally light but can still give the correct $\Omega_{\widetilde{\chi}_1^0}h^2$. The singlino and the higgsino masses are pushed towards smaller values for two main reasons: a) λ is generally large and b) the masses of singlet-like H_1 and A_1, which scale with κs, are smaller than the $H_{\rm obs}$ mass, thus forbidding κ and s from taking larger values.

The H_1 can play the role of $H_{\rm obs}$ over the complementary, and hence comparatively much larger, NMSSM parameter space, where $\tan\beta$ is not small simultaneously with large λ. However, in the NNUHM case, a nested sampling of the NNUHM parameter space (as was done in our scans) tends to direct the scans towards regions yielding H_1 solutions which are very (MS)SM-like, owing to the collider constraints imposed, given that sufficiently large m_0 and/or a_0 are allowed. In such regions, it is much harder to obtain a $\widetilde{\chi}_1^0$ with $Z_s \geq 0.05$, since λ is typically small and also since the relic density constraint is more readily satisfied by a

NNUHM parameter	Scanned range
m_0 (GeV)	500 – 2000
$m_{1/2}$ (GeV)	300 – 1000
a_0 (GeV)	−5000 – 0
$\tan\beta$	1 – 25
λ	0.15 – 0.7
κ	0.001 – 0.4
$\mu_{\rm eff}$ (GeV)	100 – 200
A_λ (GeV)	−1000 – 10000
A_κ (GeV)	−500 – 2500

(a)

NMSSM-14 parameter	Scanned range
$M_{\widetilde{Q}_3}$ (GeV)	1000 – 10000
$M_{\widetilde{U}_3}$ (GeV)	1000 – 10000
$M_{\widetilde{D}_3}$ (GeV)	1000 – 10000
$M_{\widetilde{Q}}$ (GeV)	2000 – 10000
$M_{\widetilde{L}}$ (GeV)	500 – 10000
M_1 (GeV)	500 – 10000
M_2 (GeV)	500 – 10000
A_0 (GeV)	−25000 – 0
$\mu_{\rm eff}$ (GeV)	100 – 2000
$\tan\beta$	1 – 70
λ	0.001 – 0.7
κ	0.001 – 0.7
A_λ (GeV)	0 – 25000
A_κ (GeV)	−25000 – 0

(b)

Table 2: Scanned ranges of the input parameters for (a) the NNUHM with $H_{\rm obs} = H_2$ and (b) the NMSSM-14 with $H_{\rm obs} = H_1$.

gaugino or a higgsino or their admixture. In our scans of the NNUHM for the $H_{\rm obs} = H_1$ scenario, we found only a handful of points with a non-vanishing singlino component. We therefore carried out numerical scans of the more general NMSSM-14 for this scenario only, in order to obtain a larger number of points for which $\widetilde{\chi}_1^0$ had a varying but sizeable singlino component. The scanned ranges of the NMSSM-14 parameters are given in table 2(b).

In figure 1(a) we show $\Omega_{\widetilde{\chi}_1^0}h^2$ as a function of the $\widetilde{\chi}_1^0$ mass, $m_{\widetilde{\chi}_1^0}$, for the good points obtained from our scan for the NNUHM with $H_{\rm obs} = H_2$. The colour code in the figure shows the distribution of Z_s. The maximum $\Omega_{\widetilde{\chi}_1^0}h^2$ seen for the points is 0.131, which allows for, as noted earlier, up to +10% theoretical error given the Planck measurement of 0.119. A line corresponding to the −10% error, at $\Omega_{\widetilde{\chi}_1^0}h^2 = 0.107$, is also shown. The points above this line are considered to be in agreement with the Planck measurement and are henceforth we refer to as the 'Planck-consistent' ones. We note an appreciable density of such points with $60\,{\rm GeV} \lesssim m_{\widetilde{\chi}_1^0} \lesssim 100\,{\rm GeV}$, with Z_s for them increasing with decreasing $m_{\widetilde{\chi}_1^0}$. These points are particularly interesting since, as noted from figure 1 in [87], $\widetilde{\chi}_1^0$ solutions lying within this mass range and also giving the correct $\Omega_{\widetilde{\chi}_1^0}h^2$ are almost unavailable in the MSSM. There are another two distinct sets of Planck-consistent points, one with $m_{\widetilde{\chi}_1^0} \simeq 32\,{\rm GeV}$ and the other, also an NMSSM-specific one, with $m_{\widetilde{\chi}_1^0} < 10\,{\rm GeV}$. Z_s for these points is always very large. $m_{\widetilde{\chi}_1^0}$ in this scenario does not exceed $\sim 120\,{\rm GeV}$, for reasons discussed above.

Figure 1(b) similarly shows the distribution of $m_{\widetilde{\chi}_1^0}$ for the good points from our NMSSM-14 scan for the $H_{\rm obs} = H_1$ scenario. Here also a very interesting $m_{\widetilde{\chi}_1^0}$ range can be seen for the Planck-consistent points. Neutralinos giving a good $\Omega_{\widetilde{\chi}_1^0}h^2$ and having a mass in the $\sim 500 - 1000\,{\rm GeV}$ range are also nearly impossible to realise in the MSSM, again according to figure 1 in [87]. Similarly to the $H_{\rm obs} = H_2$ scenario above, for the Planck-consistent points the singlino fraction increases as $m_{\widetilde{\chi}_1^0}$ drops, even though the typical value of the latter is much larger. The large density of points with $m_{\widetilde{\chi}_1^0} \gtrsim 1\,{\rm TeV}$ and a fairly small Z_s generally

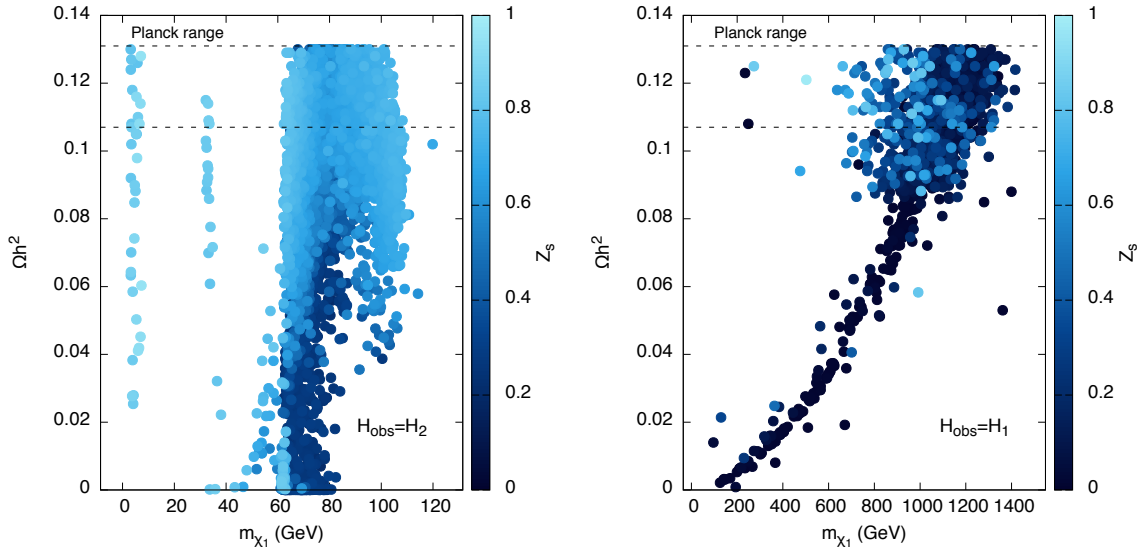

Figure 1: Relic density of the $\widetilde{\chi}_1^0$ as a function of its mass for (a) the $H_{\rm obs} = H_2$ case and (b) the $H_{\rm obs} = H_1$ case. The colour code corresponds to the singlino fraction.

is owing to the fact that a highly higgsino-dominated neutralino can easily satisfy the $\Omega_{\widetilde{\chi}_1^0}h^2$ constraint for such masses. In fact none of the points with $m_{\widetilde{\chi}_1^0} \gtrsim 1.4\,\text{TeV}$ had Z_s larger than 0.05, which is also evident from the figure.

Overall, one notices in the two figures the trend that, for a given $m_{\widetilde{\chi}_1^0}$, a larger singlino fraction results in larger $\Omega_{\widetilde{\chi}_1^0}h^2$. This is expected, since a $\widetilde{\chi}_1^0$ with a small Z_s (implying a large higgsino fraction) has a higher interaction strength and hence a higher annihilation rate compared to one with the same mass but a comparatively larger singlino fraction. There are thus some discrete $\widetilde{\chi}_1^0$ mass ranges for which the $\Omega_{\widetilde{\chi}_1^0}h^2$ obtained is consistent with the Planck observation. In between these regions no Planck-consistent neutralino solutions were obtained due to the fact that for the corresponding masses the non-singlino fraction becomes too small to obtain sufficient DM (co-)annihilation.

In the following, we shall not distinguish between points belonging to the NNUHM or to the NMSSM-14, since we are only concerned with the composition and the mass of a given $\widetilde{\chi}_1^0$. Whether a $\widetilde{\chi}_1^0$ corresponds to the $H_{\rm obs} = H_1$ scenario or to the $H_{\rm obs} = H_2$ scenario can be easily inferred from its mass.

4 Dark matter in the Sun

The description in this section follows the notation of [82]. The number of neutralinos in the Sun as a function of time, $N_\chi(t)$, is given by an evolution equation [88]

$$\frac{dN_\chi(t)}{dt} = C_\chi - A_{\chi\chi}N_\chi(t)^2 - E_\chi N_\chi(t)\,, \tag{4.1}$$

where C_χ is the neutralino capture rate (assumed to be constant), $E_\chi N_\chi(t)$ is the evaporation rate, and $A_{\chi\chi}N_\chi(t)^2$ is the annihilation rate of a pair of neutralinos. Here $A_{\chi\chi}$ is defined as

$$A_{\chi\chi} = \frac{\langle\sigma v\rangle}{V_{\rm eff}^{DM}}\,, \tag{4.2}$$

where $\langle\sigma v\rangle$ is the averaged annihilation cross section times velocity, and $V_{\rm eff}^{DM}$ is the effective volume of DM in the Sun [82]. Evaporation can be considered negligible for DM candidates above a few GeV [89], in which case $N_\chi(t) \propto \tanh(\sqrt{A_{\chi\chi}C_\chi}t)$. Thus, provided that the capture and annihilation rates are large enough, an equilibrium will be reached after a typical time scale of a few times $(A_{\chi\chi}C_\chi)^{-1/2}$, after which capture and annihilation balance each other out and the number of the DM particles is roughly constant, $N_\chi \sim \sqrt{C_\chi/A_{\chi\chi}}$. The annihilation rate is then given by the capture rate alone, $\Gamma_{\chi\chi} = A_{\chi\chi}N_\chi^2/2 = C_\chi/2$. For the Sun, most models lead to equilibrium, but MicrOMEGAs does not assume this is the case and solves the evolution eq. (4.1) numerically. The capture rate depends on the cross section for WIMP–nucleus elastic scattering and on the local density and velocity distribution in the Galaxy [88]. The default value of the local DM density, ρ_0, in MicrOMEGAs is 0.3 GeV/cm^3 and a Maxwellian velocity distribution is assumed.

The annihilation of a pair of WIMPs can lead to many different final states which decay further and eventually yield neutrinos. The energy spectrum of the neutrinos produced in the centre of the Sun is computed by MicrOMEGAs using the results of [90], for each point in the NMSSM parameter space considered. The resulting neutrino flux at the Earth is then obtained by MicrOMEGAs by computing the appropriate BRs using the NMSSM model (which in turn calls NMSSMTools). The number of events expected in IceCube is then calculated by convoluting this flux with the detector effective area and angular resolution, as explained in the following sections.

5 The IceCube and PINGU detectors

The IceCube neutrino detector [40] at the South Pole consists of one km^3 of very clear ice instrumented with 5600 optical modules arranged in 86 vertical strings. The optical modules register the Cherenkov radiation emitted by charged leptons produced in high-energy neutrino interactions in the ice. For the purpose of this paper, we are particularly interested in muons from the interactions of muon neutrinos, because such muons are observed as tracks giving a good angular resolution. Although the IceCube geometry has been optimised to detect ultra-high energy ($>$ TeV) neutrinos from potential cosmic sources with sub-degree angular resolution, its angular response of a few degrees at $\mathcal{O}(100\,\text{GeV})$ is still adequate to perform directional searches for DM. Unfortunately the energy of muon-neutrino induced events can not be precisely measured since the long muon track might not be contained within the detector volume. Electron neutrinos and tau neutrinos, on the other hand, leave localised energy depositions in the detector that, while offering much worse angular resolution, allow for a better energy measurement since they are contained in the detector. However, since we are interested in neutrinos originating in the centre of the Sun, it is important to be able to identify the direction, and we are therefore going to consider only muon neutrinos in the following. In the centre of IceCube there is a more densely instrumented sub-array called DeepCore, which is more sensitive to lower energy neutrinos, having an energy threshold around 10 GeV [91]. As we will see below, it is very important to have sensitivity to low-mass DM. In addition to the IceCube and DeepCore detectors, we consider a proposed extension called PINGU, a low-energy in-fill of about 40 additional strings with closer optical module spacing, which will have an energy threshold for neutrinos of a few GeV [41].

The efficiency of a neutrino telescope to a given signal is parametrised by the effective area for muon neutrinos, $A_{\nu_\mu}^{\rm eff}$, which is a function of the neutrino energy. The effective area is the equivalent area where the detector can detect a neutrino with 100% efficiency, and

includes the neutrino-nucleon interaction probability, the energy loss of the produced muon from the interaction point to the detector and the detector trigger and analysis efficiency. For the IceCube/DeepCore analysis we use the detector effective areas presented in [92], which were obtained from detailed simulations of the detector response within the framework of a search of IceCube data for DM in the Sun [93]. Below 40 GeV we use the PINGU effective area presented in [94]. We then have three practically independent detectors, together covering a large neutrino energy range, with little overlap between their individual coverages, as shown in figure 2 below.

6 Signal and background estimations

6.1 Expected signal from the Sun

We want to calculate the number of events that IceCube, DeepCore and PINGU can expect for the different NMSSM model points we analyse, and compare it with the number of expected background events from the direction of the Sun. The neutrino flux Φ, obtained using MicrOMEGAs from the NMSSM model, is parametrised as

$$\Phi = \frac{dN_{\nu_\mu}}{dE_{\nu_\mu}\, dA\, dt\, d\Omega}\,, \tag{6.1}$$

with neutrino energy E_{ν_μ}, area on the Earth A, time t and solid angle Ω of the sky. Ω is defined in terms of the polar angle θ and the azimuthal angle φ as $d\Omega = d\varphi\, d\theta\, \sin\theta$. MicrOMEGAs returns the neutrino and anti–neutrino fluxes separately. Even if we take "neutrino flux" to denote both neutrino and anti–neutrino flux in what follows, we treat neutrinos and anti–neutrinos separately in our calculations and use the corresponding cross sections when needed. Even though the signal from DM annihilation is independent of t, the background depends on the position of the Sun and, therefore, on t. For simplicity, we choose the coordinate system with $\theta = 0^\circ$ in the direction of the Sun. For a given detector, the total number of events observed from an incident neutrino flux is given by

$$N_{\nu_\mu} = \int dt \int_0^\infty dE_{\nu_\mu} \int_0^{2\pi} d\varphi \int_0^{\theta_{\rm cut}} d\theta \sin\theta A^{\rm eff}_{\nu_\mu}(E_{\nu_\mu})\, \Phi(E_{\nu_\mu}, \theta, \varphi, t)\,, \tag{6.2}$$

where $A^{\rm eff}_{\nu_\mu}$ is the effective area. The integral over t is done over the live time of the detector, as will be specified later. In our case of a search for DM annihilation in the Sun, the angular integral is performed over a cone that points to the Sun's position with a cut on the maximum polar angle $\theta_{\rm cut}$ to take into account the angular resolution of the detector. Φ at the detector location (Earth) will be modified by neutrino energy losses as well as oscillations on their way from the Sun. MicrOMEGAs takes care of these effects, providing the expected neutrino flux at the Earth for each signal model point considered. In a similar way, events from anti-neutrinos are calculated.

6.2 Atmospheric background

Neutrinos created in the atmosphere by cosmic ray interactions (see e.g. [95–98]) constitute an irreducible background to the signal, all year round. On top of this background, atmospheric muons produced in the same cosmic ray interactions provide an additional background that can be dealt with differently depending on the time of the year. During the antarctic summer season, when the Sun is above the horizon, neutrinos from the Sun are *downgoing*. Any search

for a solar signal is then plagued by the overwhelming atmospheric muon background, which is about seven orders of magnitude larger than the atmospheric neutrino background, depending on the declination [96, 98]. It is only through vetoing techniques (considering events starting inside the detector volume, which *must* be caused by a neutrino) that IceCube has managed to perform searches for DM in the Sun in the austral summer also. The price to pay is a significantly reduced detector volume, since part of the outer strings of the detector are used for tagging incoming atmospheric muons. Such an analysis requires access to detailed detector event information, which is beyond the scope of this work. We will thus concentrate on a "winter"-type analysis in the rest of the paper by using the corresponding effective areas from [92].

During the antarctic winter season, the Sun is below the horizon at the South Pole and neutrinos coming from it are *upgoing*, meaning that they pass through the Earth before arriving at IceCube. This provides a filter against the atmospheric muon background. The only physical background then is the atmospheric neutrino flux. There is, however, an additional background component consistent of downgoing atmospheric muons misreconstructed as upgoing. This is a background that can be minimised by clever data analyses, but a residual contamination of a few percent can always be present in the final analysis. We will assume in the rest of the paper that such misreconstructed atmospheric muon contamination can be reduced to an insignificant level in a real event-by-event analysis, and we will not consider such a background further in our calculations. Our results are then slightly optimistic, but we note that a few percent increase, ϵ, in the background would worsen the significances presented in section 7 just at the level of $1/\sqrt{1+\epsilon}$.

For our estimations of the PINGU sensitivity, on the other hand, we will not make any distinction between winter and summer periods. This is because we assume that using the surrounding IceCube detector as a veto, downgoing atmospheric muons can be effectively rejected in the summer period and the detector can be used all year round in the same way.

We calculate the expected background from state-of-the-art atmospheric neutrino flux calculations. At the energies relevant for our analysis, this background is dominated by the conventional neutrino flux from decays of pions and kaons. The prompt flux from charmed hadrons is only relevant for much higher energies. The conventional flux depends on the neutrino energy and the zenith angle. The flux prediction by Honda et al. [98] has been modified by Gaisser [99] to account for the cosmic ray knee and agrees well with the measured flux. It is used by the IceCube collaboration as a theoretical standard prediction for the conventional flux. We use this flux for our background estimates through the implementation in the code NeutrinoFlux [100]. The calculation proceeds along the same lines as for the signal estimation, that is, through the convolution of the atmospheric neutrino flux with the effective area/volume of the detector as in eq. (6.2).

7 Results and discussion

The predicted ν_μ spectra from DM annihilations in the Sun are obtained from the NMSSM model points via MicrOMEGAs, and the expected signal is calculated using the effective areas of the detectors as indicated in eq. (6.2). We consider the three independent detectors IceCube, DeepCore and PINGU, as noted above and illustrated in figure 2, each covering a different range in neutrino energy. Figure 2 also contains examples of the ν_μ spectra resulting from DM annihilation in the Sun. A few spectra with the largest signal were selected to illustrate the general features of the distributions. The irregular structure of some of the

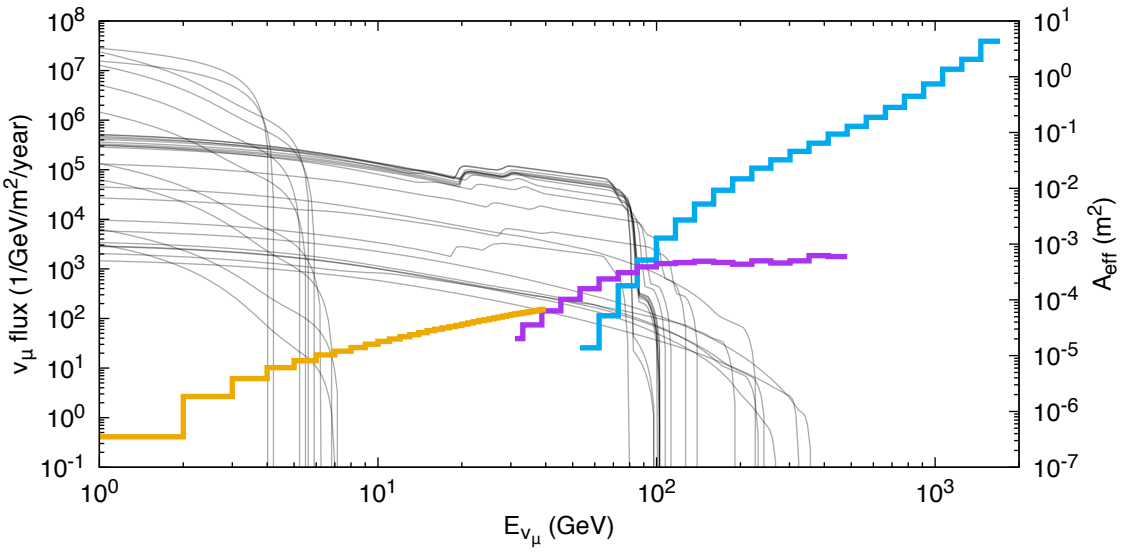

Figure 2: Examples of the ν_μ spectra (left axis) from some selected model points which result in a large statistical significance. The non-smooth features in some of the spectra originate from DM annihilation into WW or ZZ. Also shown is the energy dependence of the PINGU (orange), IceCube (blue) and DeepCore (violet) effective areas (right axis).

spectra around 30 GeV is due to the annihilation channel $\widetilde{\chi}_1^0\,\widetilde{\chi}_1^0 \to W^+W^-$, which can result in such characteristic features if the DM is heavy enough so that this channel is possible, but light enough for the spectrum to not get smoothed out [90].

For a predicted number of signal events N_s from a model and a given number of background events N_b, we estimate the significance S by the formula [101]

$$S = \sqrt{2\left((N_s + N_b)\ln\left(1 + \frac{N_s}{N_b}\right) - N_s\right)} \approx \frac{N_s}{\sqrt{N_b}}\,, \tag{7.1}$$

where the last approximation is valid for $N_s \ll N_b$. The complete expression above yields a lower S compared to the approximate one in the case of large N_s and the difference between the two amounts in our case to a maximum correction of 20%.

We integrate the signal and background over the actual live times of the detectors during one calendar year. As pointed out earlier, PINGU is assumed to take data during the whole year, since we assume that IceCube can be used as an efficient veto. IceCube and DeepCore are assumed to take data only during 152 days of the winter time as specified in table 7.1 of [92]. This lets us compare the performance of the different detectors in a more fair way.

We cut on the angle θ between the reconstructed track and the direction of the Sun as outlined in eq. (6.2) to take into account the reconstruction error for the neutrinos from the point–like source. For the signal, we assume that θ is normal–distributed around 0° with a median given by figure 7.17 in [92]. S is then maximised over θ_{cut}, with the typical optimum values being 3° for IceCube and 8° for DeepCore, while we use 20° for PINGU. The exact optimum value depends also on the specific NMSSM model point, since the angular resolution depends on the neutrino energy.

In the context of the current direct and indirect DM searches, figure 3 shows the spin-independent and spin-dependent DM-proton elastic scattering cross sections, denoted by

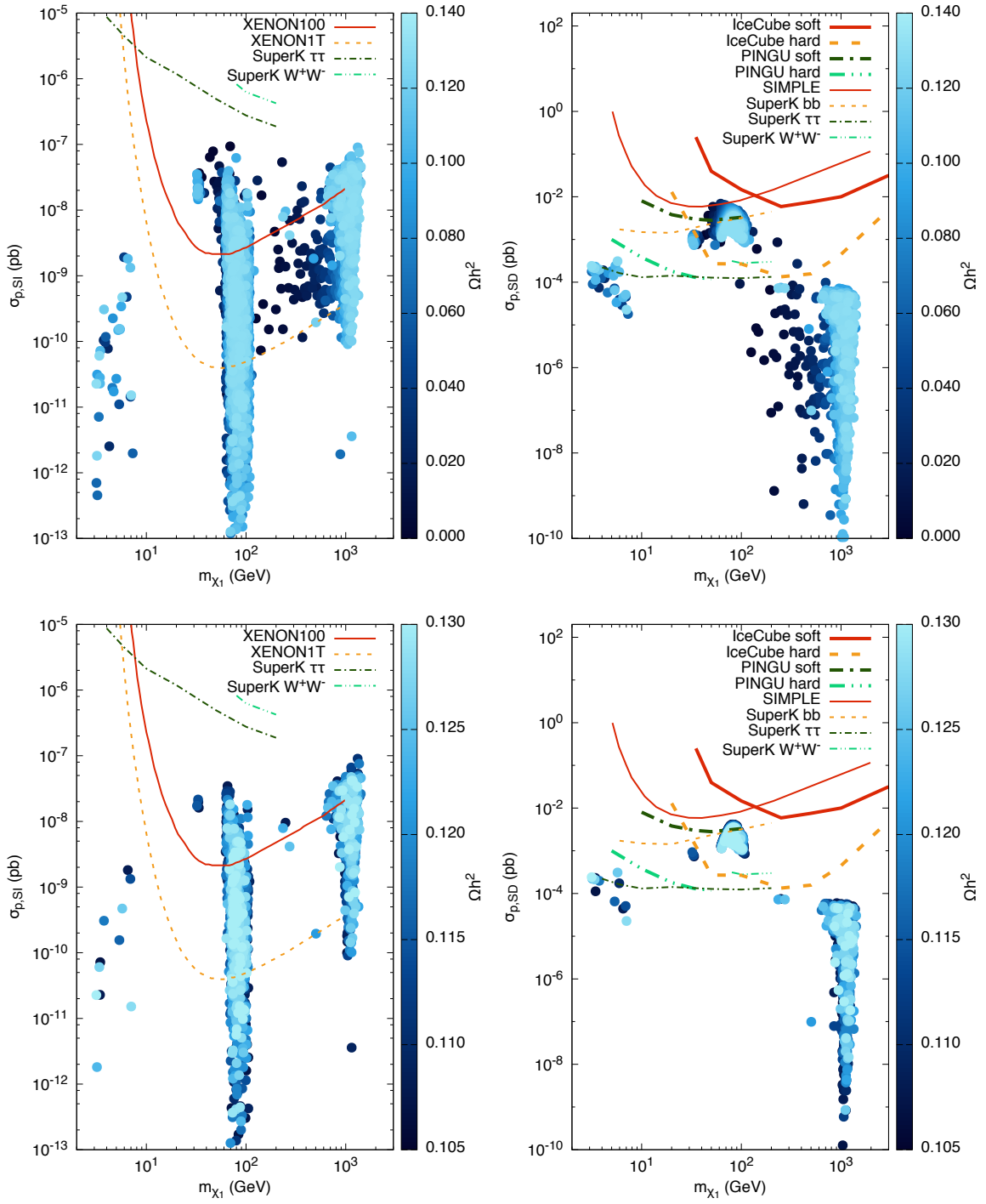

Figure 3: Scatter plots of the model points showing $\sigma_{p,SI}$ (left) and $\sigma_{p,SD}$ (right) in terms of the $\widetilde{\chi}_1^0$ mass, with the colour code corresponding to $\Omega_{\widetilde{\chi}_1^0}h^2$. The top panels contain all the good points from the scans, while the lower panels show only the model points with the predicted $\Omega_{\widetilde{\chi}_1^0}h^2$ lying within $\pm 10\%$ of the Planck measurement.

$\sigma_{p,SI}$ and $\sigma_{p,SD}$, respectively, as functions of $m_{\widetilde{\chi}_1^0}$, with the colour-code indicating the value of $\Omega_{\widetilde{\chi}_1^0}h^2$ predicted for each model point. The top panels show the complete set of good points obtained from all our scans, while the lower panels contain only the Planck-consistent (i.e., with $0.107 < \Omega_{\widetilde{\chi}_1^0}h^2 < 0.131$) subset of these points. The experimental limits shown in the left panels correspond to the current 90% CL exclusion limits from XENON100 [30] as well as the projected 90% CL limits for XENON1T [102]. In the right panels we similarly show the 90% CL exclusion limits from SIMPLE [103] and IceCube [93], as well as the projected 90% CL exclusion limits for PINGU [41]. The current limits from IceCube are shown as a guideline, but they should be interpreted with care. They were obtained under some simplifying assumptions - 100% annihilation rate into either $b\bar{b}$ (soft) or W^+W^- (hard) - and therefore can not be taken to exclude all model points lying above the corresponding lines. A real NMSSM model point has a mixture of annihilation channels and these limits would be relevant for a parameter point only if it predicts a neutralino annihilation rate almost exclusively into either $b\bar{b}$ or W^+W^-.

As can be seen from this figure, a fraction of the considered parameter points with $m_{\widetilde{\chi}_1^0} \sim 100\,\text{GeV}$ and $m_{\widetilde{\chi}_1^0} \sim 1\,\text{TeV}$ is already excluded by XENON100, and a large fraction of the remaining such points can be tested with the upcoming XENON1T experiment. The XENON1T and IceCube exclusions are, however, complementary, which we will come back to below. A note of caution here is the well-known fact that the direct and indirect detection limits on SUSY models are subject to different uncertainties from particle and nuclear physics and astrophysics. In particular, the direct detection limits are affected by large uncertainties from nuclear physics [104–106] (for recent analyses of the impact of such uncertainties on the cMSSM and MSSM parameter spaces see, e.g., [107–109]). Indirect searches for DM in the Sun are affected by several astrophysical uncertainties, mainly on the value of the local DM density, the assumed velocity distribution and velocity dispersion, although they have a more moderate effect on the final limits [110, 111]. Therefore, while we consider the points that lie above the line corresponding to XENON100 in figure 3 to be excluded, we shall anyhow include them in our discussion below, but separately from the allowed points, in order to illustrate the full complementarity of the direct and indirect searches.

The impact of IceCube, DeepCore and PINGU on the higgsino-singlino DM predictions in the NMSSM is illustrated in figures 4 and 5. The figures show the significance S defined in eq. (7.1) as a function of the $\widetilde{\chi}_1^0$ mass for the NMSSM model points after 1 calendar year. Also drawn in the figures are the lines corresponding to discovery (5σ) as well as to exclusion (2σ) after 1 or 10 calendar years, the latter aiming to highlight the model points that have not been tested by any of the detectors yet but will be after 10 calendar years of data-taking. Note that the models above the 5σ line in the plots would have probably been seen in the IceCube/DeepCore analysis presented in [93] which, even when optimised for the MSSM $\widetilde{\chi}_1^0$, does not show any other specific model dependencies, and is general enough to be sensitive to the NMSSM $\widetilde{\chi}_1^0$ as well. Such points are thus in principle already ruled out. The colour code in both the figures shows Z_s, and the model points have been sorted in such a way that a point with larger Z_s lies on top of another one with the same $m_{\widetilde{\chi}_1^0}$ and S.

Figure 4 shows the best significance, S_{Best}, obtained for a given model point by either IceCube or DeepCore. Results for PINGU will be shown later in a separate figure because PINGU has not yet started to collect data. The left panels contain only the Planck-consistent points while the right panels contain the Planck-inconsistent ones, i.e, for which $\Omega_{\widetilde{\chi}_1^0}h^2 < 0.107$. The top panels show points that are not excluded by XENON100, while the lower panels contain the complementary set, i.e., models disfavoured by XENON100. One sees in

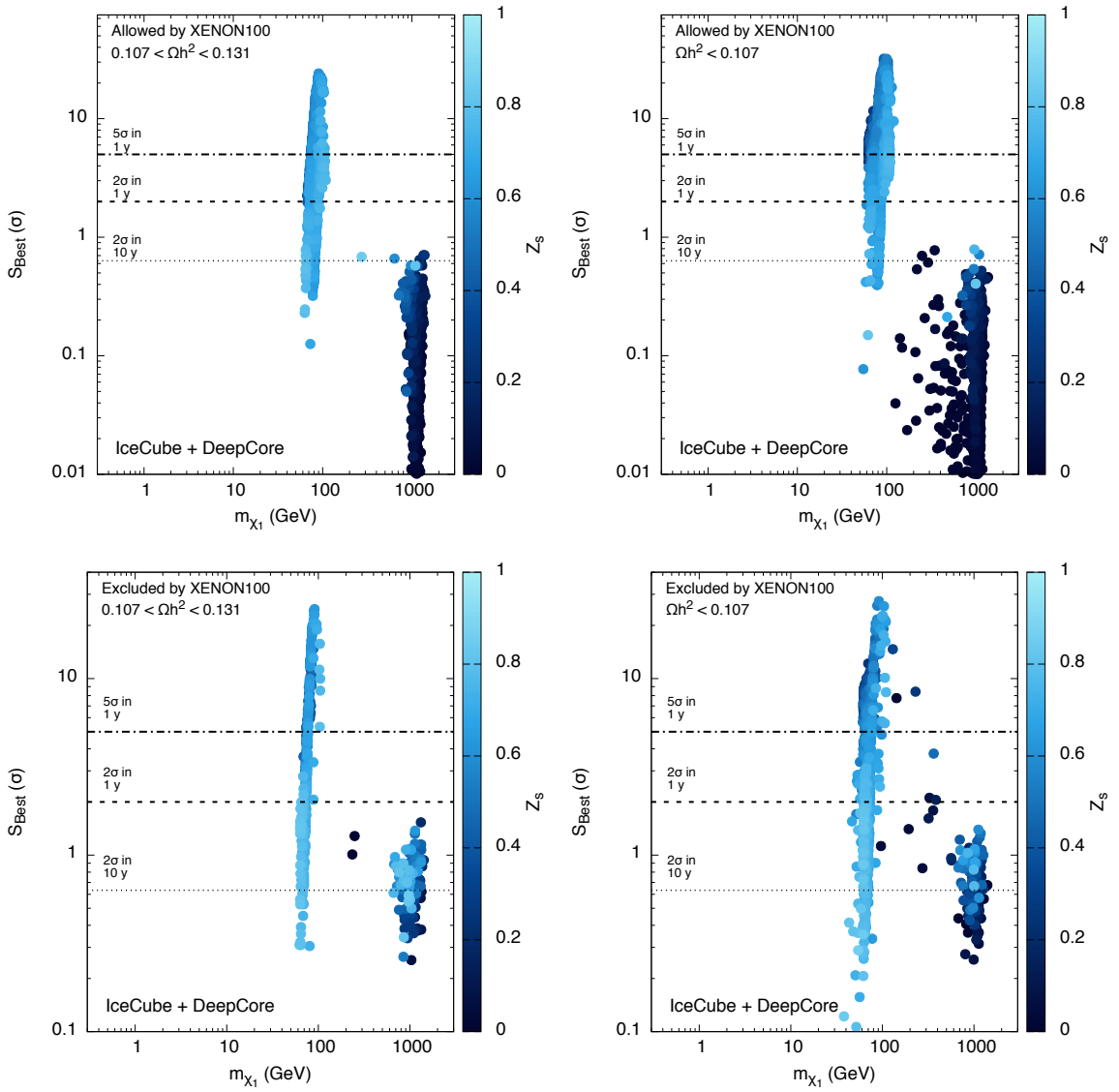

Figure 4: Overview of the maximum significance for each model point obtainable from the IceCube or DeepCore detector. The cut θ_{cut} on the angle between the tracks and the direction of the Sun is optimised for each model point. The values for the significance represent 1 calendar year of data-taking. IceCube and DeepCore are assumed to operate only during 152 days of winter, as described in the text, but PINGU, shown in later figures, operates independent of season. The colour code indicates the singlino fraction.

the figures a high sensitivity to a large number of points with $m_{\widetilde{\chi}_1^0} \sim 100\,\text{GeV}$, which can partly be traced back to the DM annihilation channel $\widetilde{\chi}_1^0\widetilde{\chi}_1^0 \to W^+W^-$ yielding a harder ν_μ spectrum for such a $\widetilde{\chi}_1^0$ mass [90]. In fact, a large fraction of the $m_{\widetilde{\chi}_1^0} \sim 100\,\text{GeV}$ points in each panel lie above the 2σ line shown. The top panels are of particular interest in this regard, since they indicate that many of these points, potentially ruled out by IceCube after just one calendar year of data-taking, were not probed by the XENON100 experiment.

Figure 5, on the other hand, shows the performance of each detector individually, but

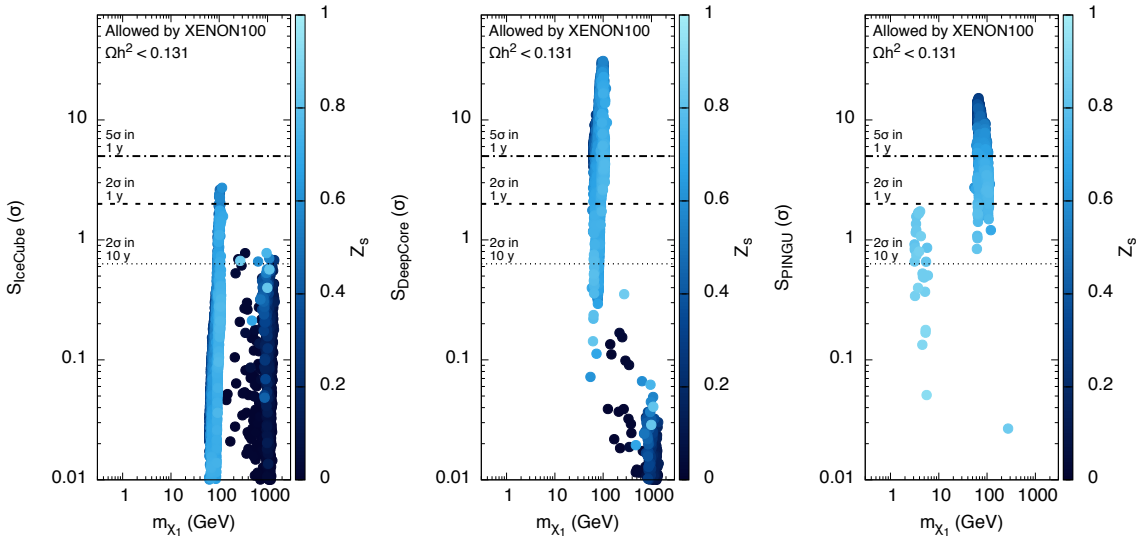

Figure 5: Expected significances at the IceCube (left), DeepCore (middle) and PINGU (right) detectors. We note that DeepCore already rules out a large fraction of the parameter space points with $m_{\widetilde{\chi}_1^0} \sim 100\,\mathrm{GeV}$ with one calendar year of data-taking (cf. figure 4), and PINGU has the potential to reach lower-mass points than those accessible with DeepCore within a few years of runtime. All points shown pass the XENON100 limits.

for model points that satisfy only the upper limit on $\Omega_{\widetilde{\chi}_1^0} h^2$ and are allowed by XENON100. We see that it is DeepCore (middle) and PINGU (right) which contribute more strongly to rejecting a large number of the $m_{\widetilde{\chi}_1^0} \sim 100\,\mathrm{GeV}$ points. As can be seen in figures 2 and 3, the $\widetilde{\chi}_1^0\widetilde{\chi}_1^0 \to W^+W^-$ annihilation channel is well covered by the DeepCore detector for this $m_{\widetilde{\chi}_1^0}$ range. Almost all the model points belonging in the $200\,\mathrm{GeV} \lesssim m_{\widetilde{\chi}_1^0} \lesssim 1400\,\mathrm{GeV}$ strip noted in the left panel (for IceCube) of figure 1(b) lie just below the line corresponding to 2σ significance after 10 years and will thus not be accessible within this timescale. Note that the inclusion of PINGU in our analysis is mainly to estimate its sensitivity to the model points with $m_{\widetilde{\chi}_1^0} \lesssim 20\,\mathrm{GeV}$. The results show that PINGU is indeed sensitive to $\widetilde{\chi}_1^0$ in the $\mathcal{O}(10\,[GeV])$ mass range, although it needs a few years of accumulated livetime. Dedicated event-based likelihood analyses, on the lines of the one presented in [112], are known to improve the sensitivity of an experiment since they use more information in a more comprehensive way, and can enhance the prospects for reaching such points with higher significance in a shorter timescale. To evaluate the effect of such an approach is, however, beyond the scope of this paper.

In figure 6 we show again the S_{Best}, but with the singlino fraction now on the x-axis and the DM mass given by the colour code. The figure further illustrates that the IceCube experiment can have a reasonable sensitivity to an abundance of points with a wide range of singlino fractions.

Finally, in figure 7 we highlight the complementarity of DeepCore/PINGU and the XENON direct detection experiment. The figure shows the $m_{\widetilde{\chi}_1^0} \sim 100\,\mathrm{GeV}$ model points which can not be excluded by the projected XENON1T 90% CL limits in a light shade on top of the ones that can be excluded, shown in darker points. As seen earlier, a subset of the points is already excluded by the available DeepCore one-year data. We note that more

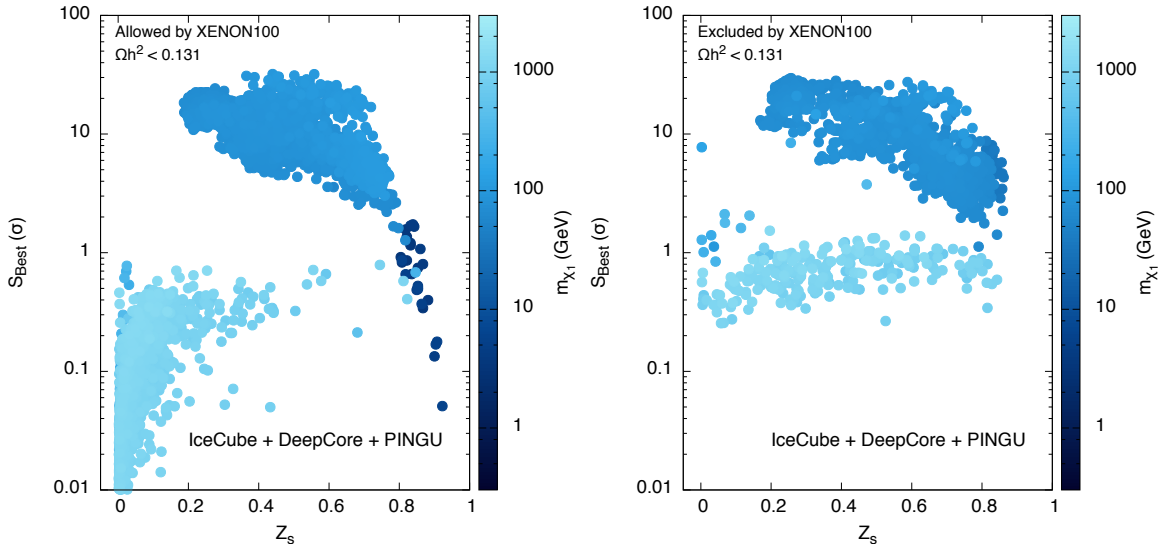

Figure 6: Best significance (from either of IceCube, DeepCore or PINGU) obtained for model points allowed (left) or excluded (right) by XENON100, against the corresponding Z_s and $m_{\widetilde{\chi}_1^0}$.

parameter space points, some of which will not be probed by XENON1T, will be testable with each subsequent year of data-taking by the DeepCore detector. The PINGU detector, when it enters operation, will also be able to test model points reachable neither by XENON1T nor by DeepCore due to the low $m_{\widetilde{\chi}_1^0}$, thus illustrating the complementarity of PINGU and DeepCore.

8 Summary and conclusions

In this article we have analysed in depth the potential of the IceCube/DeepCore detectors and the proposed low energy extension, PINGU, to probe the higgsino-singlino sector of the NMSSM. We have presented our findings from the NMSSM parameter space scans, which concentrated on model points predicting a lightest neutralino with a non-vanishing singlino fraction, and hence a non-MSSM-like dark matter candidate. In these scans we required such points to survive the most important experimental constraints from Higgs boson searches as well as from b-physics and relic density measurements.

We have used the ν_μ spectra from DM annihilation in the Sun to test the model points of our interest. We have evaluated the signal on a point-by-point basis in the NMSSM and taken into account the expected atmospheric background in the detectors considered. We have then estimated the statistical significance that can be obtained for each model point by each detector and found that a subset of all the points obtained from our scans have already been ruled out by the one-year data from the IceCube experiment, while more points will be accessible with each subsequent year of data-taking. We have found that PINGU will indeed have sensitivity to neutralino masses of the order of 10 GeV, although the detector should accumulate several years of livetime to reach a significance of 2σ for some of the points with a low $\widetilde{\chi}_1^0$ mass.

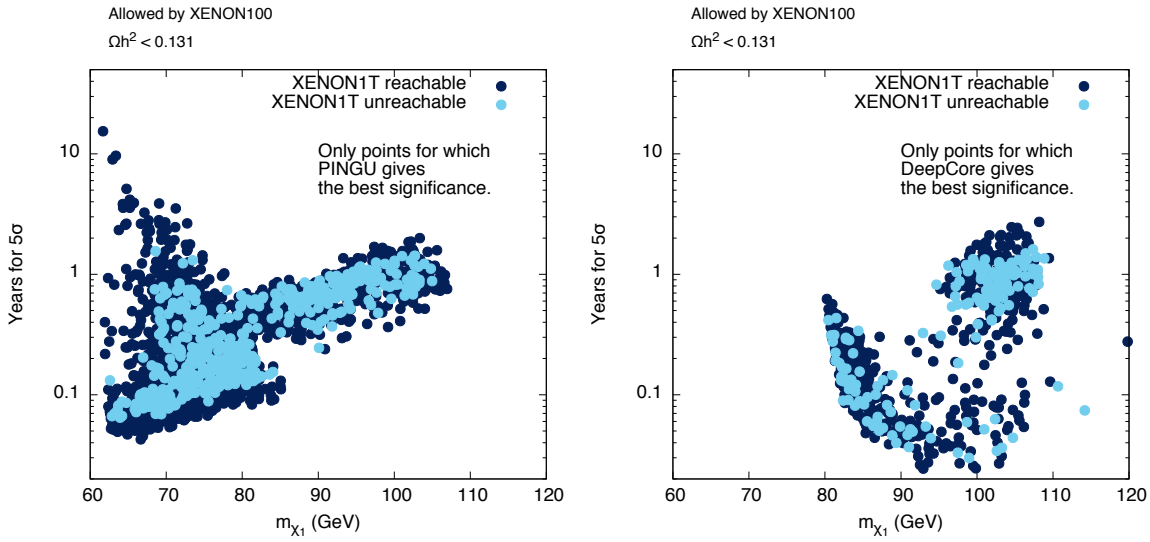

Figure 7: Number of calendar years required to reach $S = 5\sigma$ as a function of the $\widetilde{\chi}_1^0$ mass. The left plot shows only points where PINGU gives the best significance per calendar year, whereas the right plot illustrates in a similar way the case of DeepCore. Points not reachable by XENON1T with the projected sensitivity are shown in a lighter shade on top of the remaining points. We conclude that DeepCore and PINGU complement each other, and can access model points that are out of reach of the projected XENON1T sensitivity. The number of years has been extrapolated from the averaged 1-year significance. For PINGU we assume continuous data-taking over the calendar year.

We have also emphasised the complementarity of IceCube/DeepCore/PINGU searches to the ton-scale direct detection experiments, by highlighting parameter space regions that may not be probed by the latter but will be accessible at the former.

Acknowledgments

We thank Matthias Danninger for providing the numerical values of the effective areas that are shown in figure 7.17 of [92]. We thank the IceCube collaboration for providing their code NeutrinoFlux [100] that we used to compute the atmospheric neutrino flux, and David Boersma, Olga Botner, Teresa Montaruli and Anne Schukraft for help with the code. This work was funded in part by the Swedish Research Council under contracts 2007-4071, 621-2011-5107 and 621-2011-5109. SM is supported in part by the Korea Ministry of Science, ICT and Future Planning, Gyeongsangbuk-Do and Pohang City for Independent Junior Research Groups at the Asia Pacific Center for Theoretical Physics. The numerical scans were in part performed on the computational resources provided by the Swedish National Infrastructure for Computing (SNIC) at Uppsala Multidisciplinary Center for Advanced Computational Science (UPPMAX) under Projects p2013257 and SNIC 2014/1-5.

References

[1] G. Jungman, M. Kamionkowski, and K. Griest, *Supersymmetric dark matter*, *Phys.Rept.* **267** (1996) 195–373, [hep-ph/9506380].

[2] L. Bergstrom, *Nonbaryonic dark matter: Observational evidence and detection methods*, *Rept.Prog.Phys.* **63** (2000) 793, [hep-ph/0002126].

[3] G. Bertone, D. Hooper, and J. Silk, *Particle dark matter: Evidence, candidates and constraints*, *Phys.Rept.* **405** (2005) 279–390, [hep-ph/0404175].

[4] D. Hooper and S. Profumo, *Dark matter and collider phenomenology of universal extra dimensions*, *Phys.Rept.* **453** (2007) 29–115, [hep-ph/0701197].

[5] H. P. Nilles, *Supersymmetry, Supergravity and Particle Physics*, *Phys.Rept.* **110** (1984) 1–162.

[6] H. E. Haber and G. L. Kane, *The Search for Supersymmetry: Probing Physics Beyond the Standard Model*, *Phys.Rept.* **117** (1985) 75–263.

[7] P. Fayet, *Supergauge Invariant Extension of the Higgs Mechanism and a Model for the electron and Its Neutrino*, *Nucl.Phys.* **B90** (1975) 104–124.

[8] J. R. Ellis, J. Gunion, H. E. Haber, L. Roszkowski, and F. Zwirner, *Higgs Bosons in a Nonminimal Supersymmetric Model*, *Phys.Rev.* **D39** (1989) 844.

[9] L. Durand and J. L. Lopez, *Upper Bounds on Higgs and Top Quark Masses in the Flipped SU(5) x U(1) Superstring Model*, *Phys.Lett.* **B217** (1989) 463.

[10] M. Drees, *Supersymmetric Models with Extended Higgs Sector*, *Int.J.Mod.Phys.* **A4** (1989) 3635.

[11] U. Ellwanger, C. Hugonie, and A. M. Teixeira, *The Next-to-Minimal Supersymmetric Standard Model*, *Phys.Rept.* **496** (2010) 1–77, [arXiv:0910.1785].

[12] M. Maniatis, *The Next-to-Minimal Supersymmetric extension of the Standard Model reviewed*, *Int.J.Mod.Phys.* **A25** (2010) 3505–3602, [arXiv:0906.0777].

[13] S. Abel, S. Sarkar, and I. Whittingham, *Neutralino dark matter in a class of unified theories*, *Nucl.Phys.* **B392** (1993) 83–110, [hep-ph/9209292].

[14] J. Kozaczuk and S. Profumo, *Light NMSSM neutralino dark matter in the wake of CDMS II and a 126 GeV Higgs boson*, *Phys.Rev.* **D89** (2014) 095012, [arXiv:1308.5705].

[15] J. Cao, C. Han, L. Wu, P. Wu, and J. M. Yang, *A light SUSY dark matter after CDMS-II, LUX and LHC Higgs data*, *JHEP* **1405** (2014) 056, [arXiv:1311.0678].

[16] T. Han, Z. Liu, and S. Su, *Light Neutralino Dark Matter: Direct/Indirect Detection and Collider Searches*, *JHEP* **1408** (2014) 093, [arXiv:1406.1181].

[17] U. Ellwanger and C. Hugonie, *The semi-constrained NMSSM satisfying bounds from the LHC, LUX and Planck*, *JHEP* **1408** (2014) 046, [arXiv:1405.6647].

[18] **CDMS** Collaboration, R. Agnese et al., *Silicon Detector Dark Matter Results from the Final Exposure of CDMS II*, *Phys.Rev.Lett.* **111** (2013), no. 25 251301, [arXiv:1304.4279].

[19] C. Cheung, M. Papucci, D. Sanford, N. R. Shah, and K. M. Zurek, *NMSSM Interpretation of the Galactic Center Excess*, *Phys.Rev.* **D90** (2014) 075011, [arXiv:1406.6372].

[20] J. Cao, L. Shang, P. Wu, J. M. Yang, and Y. Zhang, *Supersymmetry explanation of the Fermi Galactic Center excess and its test at LHC run II*, *Phys.Rev.* **D91** (2015), no. 5 055005, [arXiv:1410.3239].

[21] L. Feng, S. Profumo, and L. Ubaldi, *Closing in on singlet scalar dark matter: LUX, invisible Higgs decays and gamma-ray lines*, *JHEP* **1503** (2015) 045, [arXiv:1412.1105].

[22] X.-J. Bi, L. Bian, W. Huang, J. Shu, and P.-F. Yin, *The interpretation for Galactic Center Excess and Electroweak Phase Transition in the NMSSM*, arXiv:1503.03749.

[23] D. Hooper and L. Goodenough, *Dark Matter Annihilation in The Galactic Center As Seen by the Fermi Gamma Ray Space Telescope*, *Phys.Lett.* **B697** (2011) 412–428, [arXiv:1010.2752].

[24] D. Hooper and T. Linden, *On The Origin Of The Gamma Rays From The Galactic Center*, *Phys.Rev.* **D84** (2011) 123005, [arXiv:1110.0006].

[25] **Fermi-LAT** Collaboration, M. Ackermann et al., *Searching for Dark Matter Annihilation from Milky Way Dwarf Spheroidal Galaxies with Six Years of Fermi-LAT Data*, arXiv:1503.02641.

[26] **DAMA, LIBRA** Collaboration, R. Bernabei et al., *New results from DAMA/LIBRA*, *Eur.Phys.J.* **C67** (2010) 39–49, [arXiv:1002.1028].

[27] **CoGeNT** Collaboration, C. Aalseth et al., *Results from a Search for Light-Mass Dark Matter with a P-type Point Contact Germanium Detector*, *Phys.Rev.Lett.* **106** (2011) 131301, [arXiv:1002.4703].

[28] **CoGeNT** Collaboration, C. Aalseth et al., *Search for an Annual Modulation in a P-type Point Contact Germanium Dark Matter Detector*, *Phys.Rev.Lett.* **107** (2011) 141301, [arXiv:1106.0650].

[29] G. Angloher, M. Bauer, I. Bavykina, A. Bento, C. Bucci, et al., *Results from 730 kg days of the CRESST-II Dark Matter Search*, *Eur.Phys.J.* **C72** (2012) 1971, [arXiv:1109.0702].

[30] **XENON100** Collaboration, E. Aprile et al., *Dark Matter Results from 225 Live Days of XENON100 Data*, *Phys.Rev.Lett.* **109** (2012) 181301, [arXiv:1207.5988].

[31] **LUX** Collaboration, D. Akerib et al., *First results from the LUX dark matter experiment at the Sanford Underground Research Facility*, *Phys.Rev.Lett.* **112** (2014) 091303, [arXiv:1310.8214].

[32] **PICO** Collaboration, C. Amole et al., *Dark Matter Search Results from the PICO-2L C_3F_8 Bubble Chamber*, *Phys. Rev. Lett.* **114** (2015), no. 23 231302, [arXiv:1503.00008].

[33] D. Das, U. Ellwanger, and A. M. Teixeira, *Modified Signals for Supersymmetry in the NMSSM with a Singlino-like LSP*, *JHEP* **1204** (2012) 067, [arXiv:1202.5244].

[34] U. Ellwanger, *Testing the higgsino-singlino sector of the NMSSM with trileptons at the LHC*, *JHEP* **1311** (2013) 108, [arXiv:1309.1665].

[35] J. S. Kim and T. S. Ray, *The higgsino-singlino world at the large hadron collider*, *Eur.Phys.J.* **C75** (2015) 40, [arXiv:1405.3700].

[36] U. Ellwanger and A. M. Teixeira, *NMSSM with a singlino LSP: possible challenges for searches for supersymmetry at the LHC*, *JHEP* **1410** (2014) 113, [arXiv:1406.7221].

[37] C. Han, D. Kim, S. Munir, and M. Park, *$\mathcal{O}(1)$ GeV dark matter in SUSY and a very light pseudoscalar at the LHC*, arXiv:1504.05085.

[38] F. Ferrer, L. M. Krauss, and S. Profumo, *Indirect detection of light neutralino dark matter in the NMSSM*, *Phys. Rev.* **D74** (2006) 115007, [hep-ph/0609257].

[39] S. Demidov and O. Suvorova, *Annihilation of NMSSM neutralinos in the Sun and neutrino telescope limits*, *JCAP* **1006** (2010) 018, [arXiv:1006.0872].

[40] **IceCube** Collaboration, A. Achterberg et al., *First Year Performance of The IceCube Neutrino Telescope*, *Astropart.Phys.* **26** (2006) 155–173, [astro-ph/0604450].

[41] **IceCube-PINGU** Collaboration, M. Aartsen et al., *Letter of Intent: The Precision IceCube Next Generation Upgrade (PINGU)*, arXiv:1401.2046.

[42] U. Ellwanger, *Radiative corrections to the neutral Higgs spectrum in supersymmetry with a gauge singlet*, *Phys.Lett.* **B303** (1993) 271–276, [hep-ph/9302224].

[43] T. Elliott, S. King, and P. White, *Supersymmetric Higgs bosons at the limit*, *Phys.Lett.* **B305** (1993) 71–77, [hep-ph/9302202].

[44] T. Elliott, S. King, and P. White, *Squark contributions to Higgs boson masses in the next-to-minimal supersymmetric standard model*, *Phys.Lett.* **B314** (1993) 56–63, [hep-ph/9305282].

[45] T. Elliott, S. King, and P. White, *Radiative corrections to Higgs boson masses in the next-to-minimal supersymmetric Standard Model*, *Phys.Rev.* **D49** (1994) 2435–2456, [hep-ph/9308309].

[46] P. Pandita, *One loop radiative corrections to the lightest Higgs scalar mass in nonminimal supersymmetric Standard Model*, *Phys Lett. B* **B318** (1993) 338–346.

[47] U. Ellwanger and C. Hugonie, *Yukawa induced radiative corrections to the lightest Higgs boson mass in the NMSSM*, *Phys.Lett.* **B623** (2005) 93–103, [hep-ph/0504269].

[48] F. Staub, W. Porod, and B. Herrmann, *The Electroweak sector of the NMSSM at the one-loop level*, *JHEP* **1010** (2010) 040, [arXiv:1007.4049].

[49] K. Ender, T. Graf, M. Muhlleitner, and H. Rzehak, *Analysis of the NMSSM Higgs Boson Masses at One-Loop Level*, arXiv:1111.4952.

[50] K. Kowalska, S. Munir, L. Roszkowski, E. M. Sessolo, S. Trojanowski, et al., *Constrained next-to-minimal supersymmetric standard model with a 126 GeV Higgs boson: A global analysis*, *Phys.Rev.* **D87** (2013) 115010, [arXiv:1211.1693].

[51] D. Kim, P. Athron, C. Balázs, B. Farmer, and E. Hutchison, *Bayesian naturalness of the CMSSM and CNMSSM*, *Phys.Rev.* **D90** (2014), no. 5 055008, [arXiv:1312.4150].

[52] A. Fowlie, *Is the CNMSSM more credible than the CMSSM?*, *Eur.Phys.J.* **C74** (2014), no. 10 3105, [arXiv:1407.7534].

[53] **ATLAS** Collaboration, G. Aad et al., *Observation of a new particle in the search for the Standard Model Higgs boson with the ATLAS detector at the LHC*, *Phys.Lett.* **B716** (2012) 1–29, [arXiv:1207.7214].

[54] **CMS** Collaboration, S. Chatrchyan et al., *Observation of a new boson at a mass of 125 GeV with the CMS experiment at the LHC*, *Phys.Lett.* **B716** (2012) 30–61, [arXiv:1207.7235].

[55] **CMS** Collaboration, S. Chatrchyan et al., *Observation of a new boson with mass near 125 GeV in pp collisions at $\sqrt{s}$ = 7 and 8 TeV*, *JHEP* **1306** (2013) 081, [arXiv:1303.4571].

[56] F. Feroz, M. Hobson, and M. Bridges, *MultiNest: an efficient and robust Bayesian inference tool for cosmology and particle physics*, *Mon.Not.Roy.Astron.Soc.* **398** (2009) 1601–1614, [arXiv:0809.3437].

[57] U. Ellwanger, J. F. Gunion, and C. Hugonie, *NMHDECAY: A Fortran code for the Higgs masses, couplings and decay widths in the NMSSM*, *JHEP* **0502** (2005) 066, [hep-ph/0406215].

[58] U. Ellwanger and C. Hugonie, *NMHDECAY 2.0: An Updated program for sparticle masses, Higgs masses, couplings and decay widths in the NMSSM*, *Comput.Phys.Commun.* **175** (2006) 290–303, [hep-ph/0508022].

[59] D. Das, U. Ellwanger, and A. M. Teixeira, *NMSDECAY: A Fortran Code for Supersymmetric Particle Decays in the Next-to-Minimal Supersymmetric Standard Model*, *Comput.Phys.Commun.* **183** (2012) 774–779, [arXiv:1106.5633].

[60] http://www.th.u-psud.fr/NMHDECAY/nmssmtools.html.

[61] U. Ellwanger, *A Higgs boson near 125 GeV with enhanced di-photon signal in the NMSSM*, *JHEP* **1203** (2012) 044, [arXiv:1112.3548].

[62] S. King, M. Muhlleitner, and R. Nevzorov, *NMSSM Higgs Benchmarks Near 125 GeV*, *Nucl.Phys.* **B860** (2012) 207–244, [arXiv:1201.2671].

[63] J.-J. Cao, Z.-X. Heng, J. M. Yang, Y.-M. Zhang, and J.-Y. Zhu, *A SM-like Higgs near 125 GeV in low energy SUSY: a comparative study for MSSM and NMSSM*, *JHEP* **1203** (2012) 086, [arXiv:1202.5821].

[64] U. Ellwanger and C. Hugonie, *Higgs bosons near 125 GeV in the NMSSM with constraints at the GUT scale*, *Adv.High Energy Phys.* **2012** (2012) 1, [arXiv:1203.5048].

[65] S. King, M. Mhlleitner, R. Nevzorov, and K. Walz, *Natural NMSSM Higgs Bosons*, *Nucl.Phys.* **B870** (2013) 323–352, [arXiv:1211.5074].

[66] T. Gherghetta, B. von Harling, A. D. Medina, and M. A. Schmidt, *The Scale-Invariant NMSSM and the 126 GeV Higgs Boson*, *JHEP* **1302** (2013) 032, [arXiv:1212.5243].

[67] **CMS** Collaboration, V. Khachatryan et al., *Precise determination of the mass of the Higgs boson and tests of compatibility of its couplings with the standard model predictions using proton collisions at 7 and 8 TeV*, *Eur.Phys.J.* **C75** (2015), no. 5 212, [arXiv:1412.8662].

[68] **ATLAS** Collaboration, G. Aad et al., *Measurement of Higgs boson production in the diphoton decay channel in pp collisions at center-of-mass energies of 7 and 8 TeV with the ATLAS detector*, *Phys.Rev.* **D90** (2014), no. 11 112015, [arXiv:1408.7084].

[69] **ATLAS** Collaboration, *Updated coupling measurements of the Higgs boson with the ATLAS detector using up to 25 fb^{-1} of proton-proton collision data*, Tech. Rep. ATLAS-CONF-2014-009, CERN, Geneva, May, 2014.

[70] **ATLAS** Collaboration, G. Aad et al., *Observation and measurement of Higgs boson decays to WW^* with the ATLAS detector*, arXiv:1412.2641.

[71] **Heavy Flavor Averaging Group** Collaboration, E. Barberio et al., *Averages of b−hadron and c−hadron Properties at the End of 2007*, arXiv:0808.1297.

[72] **Heavy Flavor Averaging Group** Collaboration, Y. Amhis et al., *Averages of b-hadron, c-hadron, and τ-lepton properties as of summer 2014*, arXiv:1412.7515.

[73] Heavy Flavor Averaging Group, 2015. http://www.slac.stanford.edu/xorg/hfag/.

[74] **LHCb** Collaboration, R. Aaij et al., *Measurement of the $B_s^0 \to \mu^+\mu^-$ branching fraction and search for $B^0 \to \mu^+\mu^-$ decays at the LHCb experiment*, *Phys.Rev.Lett.* **111** (2013) 101805, [arXiv:1307.5024].

[75] **CMS** Collaboration, S. Chatrchyan et al., *Measurement of the B(s) to mu+ mu- branching fraction and search for B0 to mu+ mu- with the CMS Experiment*, *Phys.Rev.Lett.* **111** (2013) 101804, [arXiv:1307.5025].

[76] CMS and LHCb Collaborations, *Combination of results on the rare decays $B^0_{(s)} \to \mu^+\mu^-$ from the CMS and LHCb experiments*, Tech. Rep. CMS-PAS-BPH-13-007, LHCb-CONF-2013-012, CERN-LHCb-CONF-2013-012, 2013.

[77] A. Arbey and F. Mahmoudi, *SuperIso Relic: A program for calculating relic density and flavor physics observables in Supersymmetry*, *Comput.Phys.Commun.* **176** (2007) 367–382, [arXiv:0906.0369].

[78] P. Bechtle, O. Brein, S. Heinemeyer, G. Weiglein, and K. E. Williams, *HiggsBounds: Confronting Arbitrary Higgs Sectors with Exclusion Bounds from LEP and the Tevatron*, *Comput.Phys.Commun.* **181** (2010) 138–167, [arXiv:0811.4169].

[79] P. Bechtle, O. Brein, S. Heinemeyer, G. Weiglein, and K. E. Williams, *HiggsBounds 2.0.0: Confronting Neutral and Charged Higgs Sector Predictions with Exclusion Bounds from LEP and the Tevatron*, *Comput.Phys.Commun.* **182** (2011) 2605–2631, [arXiv:1102.1898].

[80] P. Bechtle, O. Brein, S. Heinemeyer, O. Stål, T. Stefaniak, et al., *Recent Developments in HiggsBounds and a Preview of HiggsSignals*, *PoS* **CHARGED2012** (2012) 024, [arXiv:1301.2345].

[81] P. Bechtle, O. Brein, S. Heinemeyer, O. Stl, T. Stefaniak, et al., HiggsBounds – 4*: Improved Tests of Extended Higgs Sectors against Exclusion Bounds from LEP, the Tevatron and the LHC*, *Eur.Phys.J.* **C74** (2014) 2693, [arXiv:1311.0055].

[82] G. Belanger, F. Boudjema, A. Pukhov, and A. Semenov, *micrOMEGAs3.1 : a program for calculating dark matter observables*, arXiv:1305.0237.

[83] **Planck** Collaboration, P. Ade et al., *Planck 2013 results. XVI. Cosmological parameters*, arXiv:1303.5076.

[84] **Planck** Collaboration, P. Ade et al., *Planck 2015 results. XIII. Cosmological parameters*, arXiv:1502.01589.

[85] S. Profumo and C. E. Yaguna, *A Statistical analysis of supersymmetric dark matter in the MSSM after WMAP*, *Phys.Rev.* **D70** (2004) 095004, [hep-ph/0407036].

[86] K. M. Zurek, *Multi-Component Dark Matter*, *Phys.Rev.* **D79** (2009) 115002, [arXiv:0811.4429].

[87] P. Bergeron and S. Profumo, *IceCube, DeepCore, PINGU and the indirect search for supersymmetric dark matter*, *JCAP* **1401** (2014), no. 01 026, [arXiv:1312.4445].

[88] A. Gould, *Resonant Enhancements in WIMP Capture by the Earth*, *Astrophys.J.* **321** (1987) 571.

[89] A. Gould, *WIMP Distribution in and Evaporation From the Sun*, *Astrophys. J.* **321** (1987) 560.

[90] M. Cirelli, N. Fornengo, T. Montaruli, I. A. Sokalski, A. Strumia, et al., *Spectra of neutrinos from dark matter annihilations*, *Nucl.Phys.* **B727** (2005) 99–138, [hep-ph/0506298].

[91] **IceCube** Collaboration, R. Abbasi et al., *The Design and Performance of IceCube DeepCore*, *Astropart.Phys.* **35** (2012) 615–624, [arXiv:1109.6096].

[92] M. Danninger, *A search for Dark Matter Annihilations in the Sun with IceCube and Related Studies*. PhD thesis, Stockholm University, 2011.

[93] **IceCube** Collaboration, M. Aartsen et al., *Search for dark matter annihilations in the Sun with the 79-string IceCube detector*, *Phys.Rev.Lett.* **110** (2013), no. 13 131302, [arXiv:1212.4097].

[94] **IceCube** Collaboration, M. Aartsen et al., *Status of the PINGU detector*, in *Procc. of the 34th International Cosmic Ray Conference, PoS(ICRC2015)1174.*, 2015.

[95] L. Volkova and G. Zatsepin, *Prompt lepton generation—atmospheric muon and neutrino spectra at high-energies. (In Russian)*, *Sov. J. Nucl. Phys.* **37** (1983) 212.

[96] T. Gaisser and M. Honda, *Flux of atmospheric neutrinos*, *Ann.Rev.Nucl.Part.Sci.* **52** (2002) 153–199, [hep-ph/0203272].

[97] G. Barr, T. Gaisser, P. Lipari, S. Robbins, and T. Stanev, *A Three - dimensional calculation of atmospheric neutrinos*, *Phys.Rev.* **D70** (2004) 023006, [astro-ph/0403630].

[98] M. Honda, T. Kajita, K. Kasahara, S. Midorikawa, and T. Sanuki, *Calculation of atmospheric neutrino flux using the interaction model calibrated with atmospheric muon data*, *Phys.Rev.* **D75** (2007) 043006, [astro-ph/0611418].

[99] T. K. Gaisser, *Spectrum of cosmic-ray nucleons, kaon production, and the atmospheric muon charge ratio*, *Astropart.Phys.* **35** (2012) 801–806.

[100] **IceCube** Collaboration. Personal communication.

[101] G. Cowan, K. Cranmer, E. Gross, and O. Vitells, *Asymptotic formulae for likelihood-based tests of new physics*, *Eur.Phys.J.* **C71** (2011) 1554, [arXiv:1007.1727].

[102] **XENON1T** Collaboration, E. Aprile, *The XENON1T Dark Matter Search Experiment*, *Springer Proc.Phys.* **C12-02-22** (2013) 93–96, [arXiv:1206.6288].

[103] M. Felizardo, T. Girard, T. Morlat, A. Fernandes, A. Ramos, et al., *Final Analysis and Results of the Phase II SIMPLE Dark Matter Search*, *Phys.Rev.Lett.* **108** (2012) 201302, [arXiv:1106.3014].

[104] A. Bottino, F. Donato, N. Fornengo, and S. Scopel, *Implications for relic neutralinos of the theoretical uncertainties in the neutralino nucleon cross-section*, *Astropart.Phys.* **13** (2000) 215–225, [hep-ph/9909228].

[105] J. R. Ellis, K. A. Olive, and C. Savage, *Hadronic Uncertainties in the Elastic Scattering of Supersymmetric Dark Matter*, *Phys.Rev.* **D77** (2008) 065026, [arXiv:0801.3656].

[106] A. Crivellin, M. Hoferichter, and M. Procura, *Accurate evaluation of hadronic uncertainties in spin-independent WIMP-nucleon scattering: Disentangling two- and three-flavor effects*, *Phys.Rev.* **D89** (2014) 054021, [arXiv:1312.4951].

[107] R. Ruiz de Austri and C. Pérez de los Heros, *Impact of nucleon matrix element uncertainties on the interpretation of direct and indirect dark matter search results*, *JCAP* **1311** (2013) 049, [arXiv:1307.6668].

[108] A. Fowlie, K. Kowalska, L. Roszkowski, E. M. Sessolo, and Y.-L. S. Tsai, *Dark matter and collider signatures of the MSSM*, *Phys.Rev.* **D88** (2013) 055012, [arXiv:1306.1567].

[109] A. Crivellin, M. Hoferichter, M. Procura, and L. C. Tunstall, *Light stops, blind spots, and isospin violation in the MSSM*, arXiv:1503.03478.

[110] K. Choi, C. Rott, and Y. Itow, *Impact of the dark matter velocity distribution on capture rates in the Sun*, *JCAP* **1405** (2014) 049, [arXiv:1312.0273].

[111] M. Danninger and C. Rott, *Solar WIMPs unravelled: Experiments, astrophysical uncertainties, and interactive tools*, *Phys. Dark Univ.* **5-6** (2014) 35.

[112] **IceCube** Collaboration, P. Scott et al., *Use of event-level neutrino telescope data in global fits for theories of new physics*, *JCAP* **1211** (2012) 057, [arXiv:1207.0810].